Coherent Plane-Wave Compounding for Very High Frame Rate Ultrasonography and Transient Elastography

Gabriel Montaldo, Mickaël Tanter, Jérémy Bercoff, Nicolas Benech, and Mathias Fink

Abstract—The emergence of ultrafast frame rates in ultrasonic imaging has been recently made possible by the development of new imaging modalities such as transient elastography. Data acquisition rates reaching more than thousands of images per second enable the real-time visualization of shear mechanical waves propagating in biological tissues, which convey information about local viscoelastic properties of tissues. The first proposed approach for reaching such ultrafast frame rates consists of transmitting plane waves into the medium. However, because the beamforming process is then restricted to the receive mode, the echographic images obtained in the ultrafast mode suffer from a low quality in terms of resolution and contrast and affect the robustness of the transient elastography mode. It is here proposed to improve the beamforming process by using a coherent recombination of compounded plane-wave transmissions to recover high-quality echographic images without degrading the high frame rate capabilities. A theoretical model is derived for the comparison between the proposed method and the conventional B-mode imaging in terms of contrast, signal-to-noise ratio, and resolution. Our model predicts that a significantly smaller number of insonifications, 10 times lower, is sufficient to reach an image quality comparable to conventional B-mode. Theoretical predictions are confirmed by in vitro experiments performed in tissue-mimicking phantoms. Such results raise the appeal of coherent compounds for use with standard imaging modes such as B-mode or color flow. Moreover, in the context of transient elastography, ultrafast frame rates can be preserved while increasing the image quality compared with flat insonifications. Improvements on the transient elastography mode are presented and discussed.

I. Introduction

ULTRASOUND imaging has become a major medical imaging modality in the last 30 years. The main technological advance that led to its proliferation was the early development of real-time imaging capabilities. The data acquisition rate in medical ultrasonic imaging devices is only limited by the acoustic propagation velocity in the tissues. Typically, in current systems, the number of transmit events is equal to the number of scan lines to be formed, which limits the frame rate to about 30 to 40 frames per second (fps). However, increasing the frame rate in ultrasound imaging will pave the way to tremendous new applications of medical ultrasound. It will lead to future real-time 3-D imaging systems or to improved tracking of the movements of the heart during the cardiac cycle. It will also enable the visualization of transient events such as shear mechanical wave propagation for elasticity imaging or even indirect imaging of the mechanical effects of electric action potentials. High frame rate will also be used for image enhancement methods such as video integration or compounding imaging approaches.

Although its capabilities have only recently been fully developed, the concept of ultrafast echographic imaging is not new. In 1979, Delannoy *et al.* [1], [2] proposed use of parallel processing approaches to produce entire frames simultaneously from a single acoustic pulse. Their scanner was reaching a frame rate of 1000 images per second with 70 lines per frame. In 1984, Shattuck *et al.* implemented a parallel processing approach for a phased-array sector scanner enabling the simultaneous acquisition of several B-mode lines from each transmitted acoustic burst [3]. This approach was called "explososcan" by the authors, and the proof of concept was validated *in vivo*. One of the first explososcan systems was designed based on the single transmission of a "fat" ultrasonic beam and the parallel processing of 4 ultrasonic beams in the receive mode [4], [5]. This led to a system relying on a data acquisition rated increased by a factor of 4. Beyond this first successful attempt, they envisioned that this method could be, at least conceptually, extended to the imaging of a complete tomographic plane from the echoes produced by a single transmitted pulse, provided that this pulse fully illuminated the region of interest.

More than 15 years later, Fink and co-authors [6]–[8] applied successfully the concept of plane wave illuminations leading to ultrafast frame rates higher than 5000 fps. The goal was to image in real time the transient propagation of shear mechanical waves in human tissues for the assessment of local viscoelastic properties, a technique dubbed "transient elastography." This ultrafast approach led to the first experimental in-vivo investigation for breast cancer diagnosis [9]. Finally in 2004, by combining this ultrafast imaging modality with a remote palpation induced by the radiation force of ultrasonic focused beams, they provided an efficient way to build viscoelasticity maps of human tissues using a conventional echographic probe, the so-called supersonic shear imaging (SSI) technique [10], [11].

Another approach for reaching a high frame rate that used nondiffracting beams was proposed by Lu and Greenleaf in the early 1990s [12]–[14]. Following these pioneer works, Lu developed a theory in which a pulsed plane wave was used in transmission, and limited-diffraction array beam weighting was applied in reception to produce a spatial Fourier transform of the object function for 3-D image reconstruction. Later, he proposed the use of spatial compounding with different steered plane waves or limited diffraction beams added in a coherent way (enhancing resolution) or added in an incoherent way (reducing speckle) [15]–[17].

Ultrasound compound imaging for medical imaging dates back to the early 1980s [18] and has been widely studied in the last decade [19], [20]. To date, this concept of compound imaging is mainly associated with an incoherent addition of several image frames in an attempt to cancel out random variations (noise) and hence increase the signal to noise ratio [20], [21]. The reported benefits of image compounding in ultrasonography include reduced speckle, reduction in artifacts (clutter, shadowing, echo drop-out), higher contrast, and better visibility of lesion margins (making lesions more conspicuous). The "incoherent" terminology is related to the summation method that acts on the intensity images to smooth the speckle noise.

Contrary to incoherent compound imaging, coherent wave compounding has not been extensively studied. It consists of the recombination of backscattered echoes from different illuminations achieved on the acoustic pressure field (as opposed to the acoustic intensity for the incoherent case). Although the concept has already been proposed [22] and mentioned in the context of limited diffraction beams [17], to date, no extensive work has been done to study its performance and advantages. We propose in this paper a theoretical model quantifying the performance of the coherent plane-wave-compounding approach. The interesting finding reported here is that the number of insonifications needed to achieve a given image quality is significantly lower than for classical approaches to B-mode. This characteristic opens new potential applications to the method such as transient elastography and fast color-flow imaging.

Coherent plane-wave compounding of images obtained with different angles presents strong conceptual analogies with the synthetic aperture method [23], [24]. In the synthetic aperture approach, the ultrasonic array is fired element by element, and the complete set of impulse responses between each transmit-and-receive element is recorded. It is then possible to post-process these data to generate a synthetic image relying on both transmit-and-receive focusing for each pixel of the image. It has been intensely discussed in the literature whether synthetic imaging could give better images than conventional B-mode images, and how they will be affected by tissue motion and limited signal-to-noise ratio. A fundamental problem in synthetic aperture imaging is the poor signal-to-noise ratio in the images, because a single element is used for emission. This gives much lower emitted energy compared

with using the full aperture in conventional imaging and, therefore, limits the depth of penetration.

Coherent plane-wave imaging solves at least partially these limitations of synthetic aperture imaging. First, the transmission of a plane wave on the complete array generates a much higher wavefield than in the synthetic aperture approach. Second, as it will be shown in this paper, the reconstruction of high-quality echographic images in a small amount of time enables measurement of tissue displacement or flow-imaging processing.

As already mentioned, in the SSI, the ultrafast frame rate is reached by limiting the illumination to a single plane-wave transmission and storing the backscattered signals in RAM memory. The image formation is then reduced to a conventional beamforming approach in the receive mode. Consequently, a single insonification is sufficient to produce an echographic image. The time between 2 consecutive images is only limited by the propagation time in tissues. As an example, the acquisition of 50 mm depth images can be theoretically produced at a frame rate of ∼10 Kf/s. Due to the lack of transmit focusing, the echographic image quality is of course degraded in terms of contrast and resolution, and such degradation has consequences for the robustness of the elastography mode. In a previous work [25], we demonstrated the interest of incoherent plane-wave compounding at ultrafast frame rates for the estimation of transverse tissue displacements in transient elastography. In that case, the goal was to improve the estimation of lateral motion by increasing the number of independent speckle noise patterns used for the speckle tracking estimation. As speckle patterns recorded for different illumination angles were decorrelated, the variance of lateral motion estimates was improved following a square root dependence versus the number of angles. In this article, we propose investigation of the concept of coherent plane-wave compounds for improving echographic image quality without resorting to very high frame rate capabilities. The new imaging sequence is based on the coherent summation of ultrafast images obtained from plane wave transmissions at different angles.

The paper is organized as follows: In Section II, a theoretical comparison is derived between the plane-wave compounding approach and an optimal multifocus imaging technique relying on both transmit-and-receive focusing for each point of the final image. We demonstrate that the plane-wave compounding approach can reach the optimal multifocus image quality using a small number of plane wave transmissions while preserving high frame rates. In Section III, a quantitative experimental comparison of both approaches is presented with a careful comparison in terms of resolution, contrast, signal to noise, and frame rates. In Section IV, the number of transmissions is drastically reduced to reach ultrafast frame rates (higher than 1000 fps), and the concept is applied to transient elastography. Experiments are provided and improvements in the elasticity-imaging mode are presented.
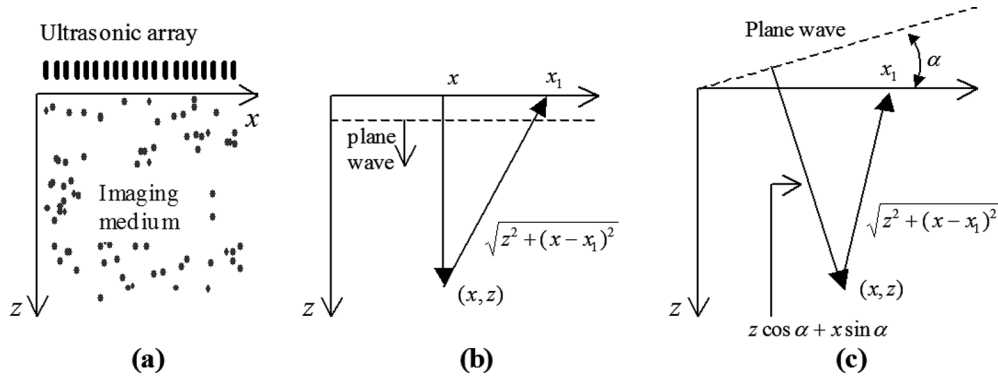
Fig. 1. (a) Axis convention, (b) time delays for a plane wave insonification, and (c) time delays for a plane wave of angle α.
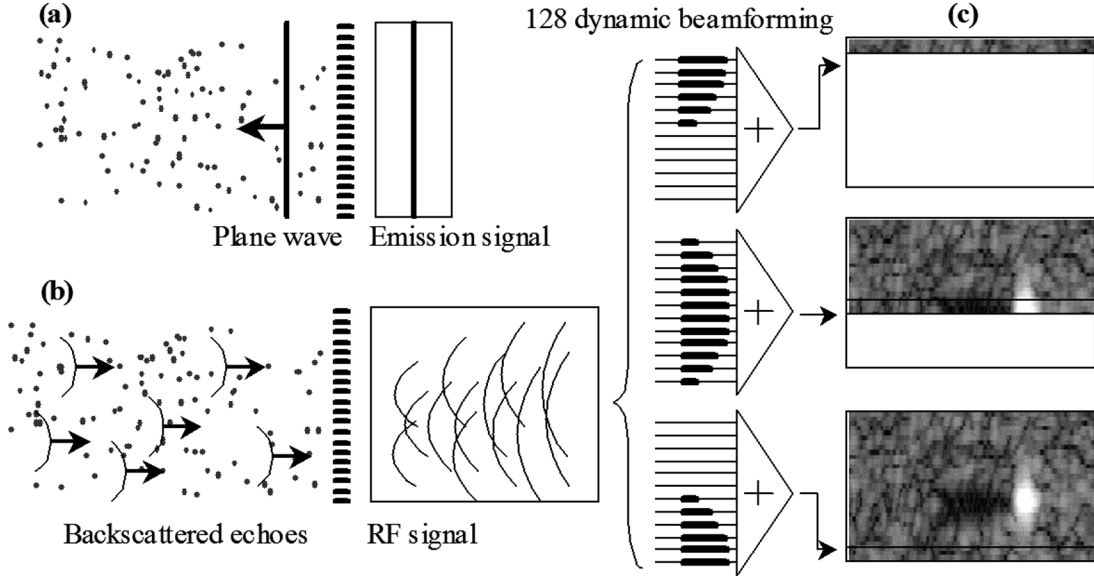

Fig. 2. Schematic representation of the single transmit plane wave method: (a) The ultrasonic array insonifies the medium using a plane wave transmission. (b) The backscattered RF signals are recorded by the transducer array. (c) The beamforming procedure consists in applying time delays laws and summations to the raw RF signals to focus in the receive mode. Contrary to standard ultrasonography, each line of the image is calculated using the same RF data set but a different set of time delays.

II. THEORY

A. The Single Plane Wave Imaging Mode

A typical configuration of ultrasonic imaging systems is presented in Fig. 1(a). A linear array made of n_t transducers (typically 128) are placed directly in contact with the medium of interest. The x direction is parallel to the array, and z is the depth direction in the imaging medium.

In ultrafast imaging, one needs to produce an entire frame simultaneously from a single acoustic pulse with parallel processing. The most obvious way to insonify the medium is to transmit a large beam made of a unique pulsed plane wave; see Fig. 2(a). Then, this wave is backscattered by the heterogeneities of the medium and the array receives the echo signals $RF(x_1,t)$; see Fig. 2(b). Because we do not have any focusing for the transmit beam, the image resolution is obtained only by a parallel processing during the reception mode by adding coherently the echoes coming from the same scatter.

For a plane-pulsed wave, Fig. 1(b) shows that the traveling time to the point (x,z) and back to a transducer placed in x_1 is given by

$$\tau(x_1, x, z) = \left(z + \sqrt{z^2 + (x - x_1)^2} \right)/c, \qquad (1)$$

where c is the speed of sound that we assumed to be constant in the medium.

Each point (x,z) of the image is obtained by adding coherently the contribution of each scatter, i.e., delaying the $RF(x_1,t)$ signals by $\tau(x_1,x,z)$ and adding them in the array direction x_1

$$s(x,z) = \int_{x-a}^{x+a} RF\left(x_1, \tau(x_1,x,z) \right) dx_1. \qquad (2)$$

The aperture $2a$ must take into account only the elements that contribute to the signal. This aperture $2a$ is always
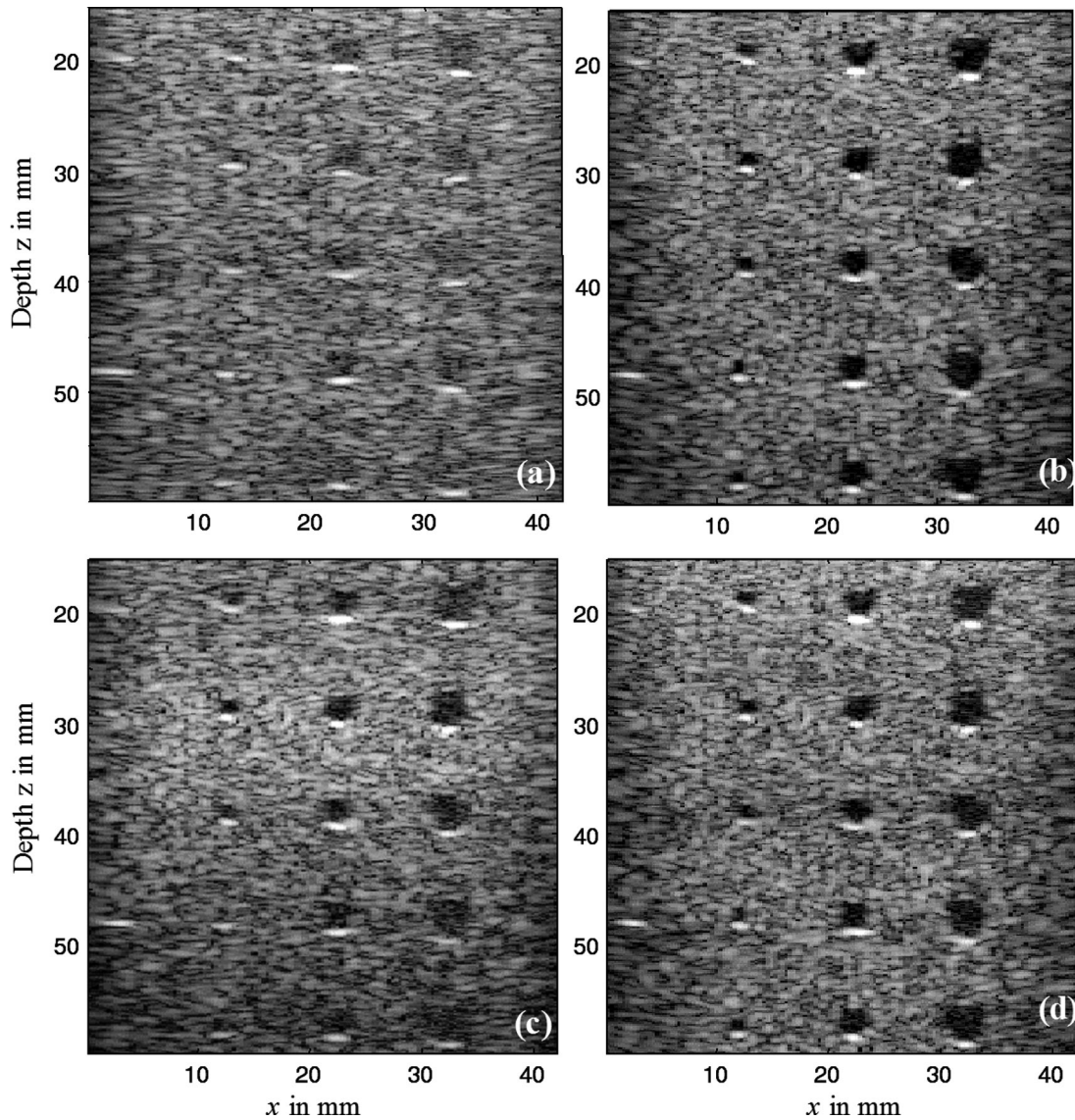
Fig. 3. (a) B-mode image obtained using a single plane wave transmission. (b) Coherent plane wave compound using 71 angles separated 0.47°; value given by (12). (c) Standard monofocal image using a single focal depth at 30 mm. (d) Multifocal image using 4 successive focal depths. Images performed with a 128-element array of 4.5 MHz, 60% bandwidth, pitch of 0.33 mm, F number of 1.75 both in emission and in reception, the lateral scan is done at $\lambda/2$. There is no apodization in emission and in reception for either the focused or the compound method.

lower than the total length of the array L, and it can be expressed by the F-number defined as

$$F = z/2a. \qquad (3)$$

The useful F-number depends on the directivity of the array (typical values are between 1 to 2) and ideally must be constant in the entire image.

In dynamic beamforming, the delays τ are computed at each depth z to produce a complete line of the image. The final image is obtained by producing in parallel n_e dynamic beamformings with the same RF data, one for each line of the image; see Fig. 2(c).

The insonification with a single plane wave provides the fastest method, with a frame rate of nearly 10 kf/s, but with a significant reduction in the image quality. Fig. 3(a)

shows an image of a calibration phantom with anechoic inclusions embedded in a homogeneous speckle environment obtained with a single plane wave.

All the images in the article were produced with a 128-element array working at 4.5 MHz central frequency, 60% bandwidth, and pitch of 0.33 mm. The last 4 channels of the electronics did not work, and the array was reduced to 124 elements. The F number is 1.75 in all the methods. The lateral scan in the beamforming is always at $\lambda/2 = 0.17$ mm with a total of 256 lines. There is no apodization in emission and in reception.

As shown on the image, the contrast is low: the inclusions are only –10 dB lower than the background. To improve the image quality, image compounding is proposed to obtain plane waves of different angles in a coherent way to resynthesize the transmit focusing.

B. The Coherent Plane Wave Compound

If we send a plane wave with inclination α as in Fig. 1(c), the time to go to a point (x,z) in the medium is

$$\tau_{ec}(\alpha, x, z) = (z\cos\alpha + x\sin\alpha)/c, \qquad (4)$$

and the time to come back to a transducer placed in x_1 is

$$\tau_{\text{rec}}(x_1, x, z) = \sqrt{z^2 + (x - x_1)^2}/c. \qquad (5)$$

The total 2-way travel time τ for a plane wave insonification, is then

$$\tau(\alpha, x_1, x, z) = \tau_{ec} + \tau_{\text{rec}}. \qquad (6)$$

Then an image is obtained in the same way as shown in (2), but with the new delays from (6).

The image quality can be upgraded by compounding coherently the images obtained with several plane waves of different angles. We choose a set of n plane waves with inclination angles α_i, $i = 1, \ldots, n$. For each plane wave, an image is built following the previous procedure. All images are then added coherently to obtain a final compounded image. Note that the addition is produced without taking the envelope of the beamformed signals or any other non-linear procedure to ensure a coherent addition.

Sending n plane waves requires more time and reduces the frame rate by a factor n_k. If the plane wave recurrence reaches a frame rate of 10 kf/s, the transmission of 10 compound plane waves with different angles will give a frame rate of 1 kf/s, which nearly corresponds to the frame rate limit for transient elastography. A detailed analysis of the compromise between quality and frame rate is presented in Section IV.

Fig. 3(b) shows an example of a coherently compounded image using 71 plane wave transmissions with a separation of 0.47° between each angle. As one can notice, it has a much better contrast than the image obtained using a single plane wave. To quantify this improvement, this coherently compounded image must also be compared with the multifocus image that corresponds to the standard method used in conventional ultrasound scanners.

C. Standard Sequential Imaging Using Focused Transmit Beams

In the standard sequential imaging procedure, the complete image is obtained line by line. For each line of the image corresponding to a lateral position x_f, the medium is insonified with a narrow beam obtained with cylindrical transmitted delays that focuses a wave on a given point (x_f, z_f). The 2-way delay for the scatters placed in the line x_f is

$$\tau(x_1, x_f, z) = \left(z + \sqrt{z^2 + (x_f - x_1)^2}\right)/c. \qquad (7)$$

A line of the image at position x_f, is produced by using a dynamic focusing in reception, and the complete image is built by scanning with a set of focused waves at different lateral positions x_f. The reconstructed image is optimal only around each focal depth z_f, in a limited region of the medium corresponding to the depth of field of each transmitted focus beam. Fig. 3(c) shows an example of an image obtained with only one focal depth in transmit. The image is good only near the transmit focal area, and it is progressively degraded outside. To improve the image quality, different transmit focal depths are used, and the final image is obtained using a recombination of these partial images corresponding to various depths.

Fig. 3(d) shows a multifocus image obtained with 4 focal depths. The comparison with the single focus image in Fig. 3(c) clearly exhibits an improvement of the image. To provide the optimal multifocus image, the transmit focal depths must be separated by a maximal distance corresponding to depth of field $\Delta z = 7\lambda F^2$ [26]. In such a configuration, the frame rate is drastically reduced, and in practice, no more than 4 focal depths are used, as in the example of Fig. 3(d). To compare the performances with the compound method, the F number is the same (1.75) and the lateral scan was done at $\lambda/2 = 0.17$ mm. There is no apodization in emission and in reception for either the focused or the compound method. Of course, classical apodizations can be implemented, but the improvements must be similar in both methods.

With a single focus per line, a frame rate of approximately 100 frames/s can be achieved for a 50 mm depth image. Using 4 focal depths, we achieved a frame rate of ~25 frames/second. To get an image of optimal resolution along all the depths, we need at least 12 focal depths, leading to a limit of only 8 frames/second.

In the next section, it is demonstrated that, using the coherent plane-wave compound method, the optimal image quality can be obtained using a reduced number of plane-wave insonifications. It is shown that the resolution, contrast, and signal-to-noise ratio are the same as in the optimal multifocus image but with frame rates higher than 200 f/s. Furthermore, we demonstrate that the image quality obtained, keeping the required frame rate for transient elastography (1 kHz), is comparable to a standard monofocus B-mode imaging.

D. Theoretical Comparison Between the Coherent Compounding Approach and the Optimal Multifocus Imaging Technique

In the multifocus method, we have a clear separation between transmit (achieved by the real transmission of focused beams in the medium) and receive focusing (achieved by the beamforming operation). In the coherent compound approach, the emission is composed of n_k plane waves that are fired one by one, and the images of each plane-wave insonification are added coherently. This last addition of images generates a posteriori a synthetic focusing in the transmit mode. Thus, the focusing operation in
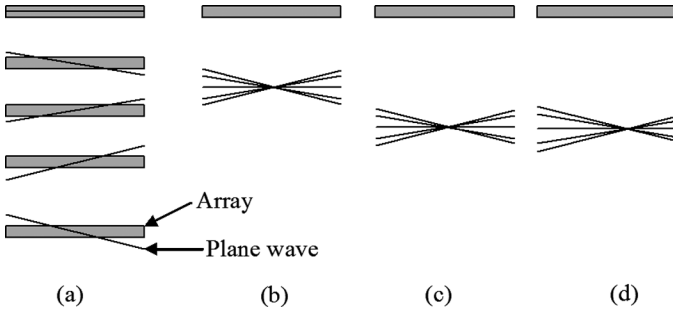
Fig. 4. (a) Individual plane waves send with the compound method. (b), (c), (d) The addition of the plane waves with the adequate delays enables focus at different depths and laterally. This focusing is performed synthetically. If this synthetic focusing is the same as in the standard focusing method, the final image must have the same quality in both methods.

transmit-and-receive mode are mixed, which makes the comparison between the 2 imaging methods a little more complex.

If $p_c^i(x,z,t)$ are the plane waves of pressure with inclination α_i, the image in a point (x_f, z_f) of the medium is produced with a combination of these waves. In Appendix A, we demonstrate that the image of a point (x_f, z_f) with the compound method is the same as the image we can obtain illuminating the medium with a unique wave

$$p_c(x,z,t;x_f,z_f) = \sum_i p_c^i(x,z,t + \tau_{ec}^i(\alpha_i, x_f, z_f)), \quad (8)$$

where τ_{ec}^i is the travel delay to the point (x_f, z_f) presented in (4).

We can interpret this new unique wave as a the synthetic wave that focuses in the point (x_f, z_f).

If this wave $p_c(x,z,t;x_f,z_f)$ is a cylindrical one, we obtain an equivalence between the standard focusing method and the compound method.

Fig. 4 shows a schematic representation of the synthetic wave; the compound method sends individual plane waves as in Fig. 4(a). Using the delays $\tau_{ec}^i(\alpha_i, x_f, z_f)$ these plane waves interfere constructively in the focal point (x_f, z_f); see Fig. 4(b). With the same set of waves, we can focus at different depths, as in Fig. 4(c), and laterally, as in Fig. 4(d).

If we demonstrate that the synthetic focal spots are identical to the focal spot of a cylindrical wave, we can conclude that the 2 methods generate the same image.

Intuitively, Fig. 4 shows that the equivalence between the synthetic and cylindrical focal spot is true if the synthetic wave is the plane wave decomposition of the focused wave. We perform the demonstration in the monochromatic case, and it is later generalized to a realistic transducer relying on a large bandwidth.

To demonstrate this equivalence, we write the explicit expression of the monochromatic plane waves $p_c^i(x,z,t)$ of inclination α_i

$$p_c^i(x,z,t) = p_0 \exp j(xk_x^i + zk_z^i - \omega t),$$
$$k_x^i = k_0 \sin\alpha_i, \quad k_z^i = k_0 \cos\alpha_i, \quad k_0 = 2\pi/\lambda. \quad (9)$$

A first problem is to choose the set of angles α_i. This question can be answered considering that a linear array of n_t elements with a spacing dx between elements generates a sampling in the x direction. The spatial sampling frequency is $1/dx$, we prefer to express it in the angular spatial frequency (that gives the k space directly) as $k_{\text{sam}} = 2\pi/dx$. The total spatial frequency spectrum available with this sampling frequency is within the range $(-1/2k_{\text{sam}}, 1/2k_{\text{sam}}) = (-\pi/dx, \pi/dx)$. In this interval we have n_t independent spatial frequencies given by

$$k_x^i = \frac{2\pi}{dx}\frac{i}{n_t}, \quad i = -n_t/2, \ldots, n_t/2 - 1. \quad (10)$$

As the total length of the array is $L = n_t dx$, the set of spatial frequencies in the x direction is

$$k_x^i = i2\pi/L, \quad i = -n_t/2, \ldots, n_t/2 - 1. \quad (11)$$

Using the definition of k_x^i (9) the angles are given by

$$\alpha_i = \arcsin(i\lambda/L) \approx i\lambda/L, \quad i = -n_t/2, \ldots, n_t/2 - 1. \quad (12)$$

The transmission of n_i plane waves with this angles guarantees that no information is lost in the angular spectrum of the synthetic set of transmitted waves. However, in some cases, the transmission of the complete set of n_i angles is not required because the directivity of the array limits the use of high spatial frequencies.

After defining the angles, we return to the original problem of the equivalence between the synthetic emission wave and the cylindrical focusing. Replacing the delays 4 in (8) and (9), we obtained the result that the synthetic wave is

$$p_c(x',z',t) = \sum_{i=-n/2}^{n/2-1} p_0 \exp j(x'k_x^i + z'k_z^i - \omega t), \quad (13)$$

where $x' = x - x_f$ and $z' = z - z_f$ are the coordinates centered at the focal point (x_f, z_f). In this equation, the total number of angles n is not defined, and it must be adjusted to generate the same focusing as the standard method.

From the diffraction theorem, knowing the field at given depth is enough to know it in all the space, we can choose to study at the focal depth $z = z_f$ then

$$p_c(x',t) = \sum_{i=-n/2}^{n/2-1} p_0 \exp j(x'k_x^i - \omega t). \quad (14)$$

Replacing k_x^i by (10) we arrive at a geometrical series that can be added explicitly

$$p_c(x',t) = p_0 \frac{j2\sin(x'n\pi/L)}{[\exp(jx'2\pi/L)-1]}\exp(-j\omega t). \qquad (15)$$

The denominator can be approximated by $\exp(jx'2\pi/L) - 1 \approx jx'2\pi/L$ and (15) becomes a sinc function

$$p_c(x',t) = p_0 n \, \text{sinc}(x'n\pi/L)\exp(-j\omega t). \qquad (16)$$

In the standard method, a cylindrical wave focusing at depth z_f and aperture $(-\alpha, \alpha)$ generates a similar sinc function in the focal plane

$$p_f(x,t) = p_0 g(z_f)\,\text{sinc}(xak_0/z_f)\exp(-j\omega t), \qquad (17)$$

where $g(z_f)$ is the gain of antenna given by

$$g(z_f) = 2a/\sqrt{\lambda z_f}. \qquad (18)$$

Comparing (16) with (17) we can deduce that the number n of angles that we need to have the same sinc function is

$$n = \frac{ak_0 L}{z_f \pi} = \frac{L}{\lambda F}. \qquad (19)$$

As an example, the array used in this article has 124 active elements with pitch $dx = \lambda$ and a F-number of 1.75. From the (19) it is enough to use 71 plane waves insonifications to obtain the same focusing quality as the optimal multifocus. This typical value is used throughout this paper to compare with the standard method.

Another interpretation of this section is that the spatial spectrum of the focused wave (the sinc function) is a rectangle $(-k_0/2F, k_0/2F)$ that we can see in Fig. 5. As each plane wave $p_0 \exp j(xk_x^i + zk_z^i - \omega t)$ generates a unique spatial frequency k_x^i, we must add all the spatial frequencies that are in the rectangle $(-k_0/2F, k_0/2F)$ with the same weigh. This calculation was performed in the monochromatic case. For the general case of a wideband wavefield, the focal spot corresponding to (17) is not exactly a sinc function, and the spectrum is not exactly a rectangle (see Fig. 5). Then we must add the plane waves with a different weight in the edge of the spectrum to take into account the band of the transducer.

To give an example, in Appendix B the calculation of the spatial Fourier spectrum $P_f(k_x)$ is derived from a broadband signal of temporal spectrum $B(\omega)$ and it is

$$P_f(k_x) = \int\limits_{k_x c z_f / a}^{+\infty} B(\omega)\,d\omega. \qquad (20)$$

We can illustrate (20) in the particular case of a Gaussian pulsed signal with a bandwidth $\Delta\omega$ centered in ω_0
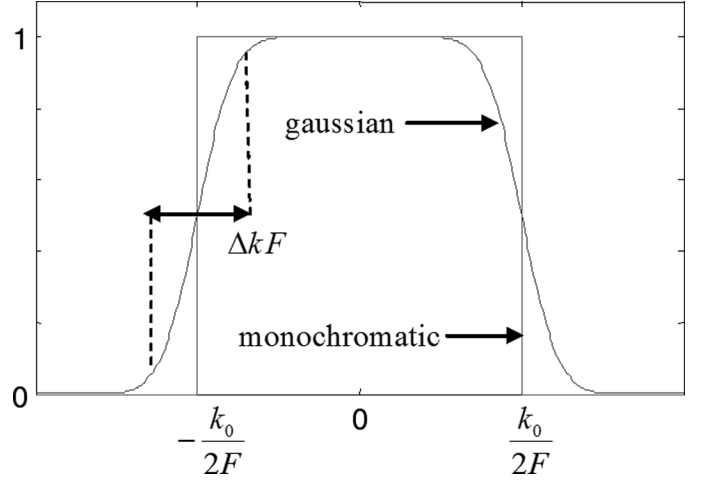

Fig. 5. The spatial spectrum of the focal spot is a rectangle for a monochromatic wave, but for a pulsed wave, it has smooth edges. The plane waves must be added with a weight corresponding to the amplitude of the spectrum to take into account the frequency bandwidth of the wave.

$$B(\omega) = \frac{1}{\Delta\omega\sqrt{2\pi}}\exp\left[\frac{-(\omega-\omega_0)^2}{2\Delta\omega^2}\right]. \qquad (21)$$

The integration of (19) gives the error function

$$P_f(k_x) = \Phi\left(\frac{\left|k_x\right|\frac{z_f}{a} - k_0}{\Delta k}\right), \qquad (22)$$

with $\Delta k = \Delta\omega/c$. In that case, the edges of the rectangle in the spatial Fourier transform are smoothed in a section $\Delta k F$ as in Fig. 5.

This example shows that the monochromatic model can be extended to a wideband case taking into account a weight $P_f(k_x^i)$ before the addition of the images. From a practical point of view, we found that the exact shape of the transducer band is not critical. Using different shapes for the band of the transducers generates only small differences in the contrast of the images. The weights in the experiments are calculated with (22), with a Δk of $0.3k_0$.

III. Experimental Quantitative Comparison

The usual criteria for the characterization of an imaging method are the resolution, the contrast, the frame rate, and the SNR level. In this section, we compare the multifocal and the compound imaging approaches.

A. Lateral Resolution

An ultrasonic image is usually depicted as obtained through a linear filter or point-spread function (PSF) that links the object to image $o(x_1,z_1)$ with the obtained image $s(x,z)$
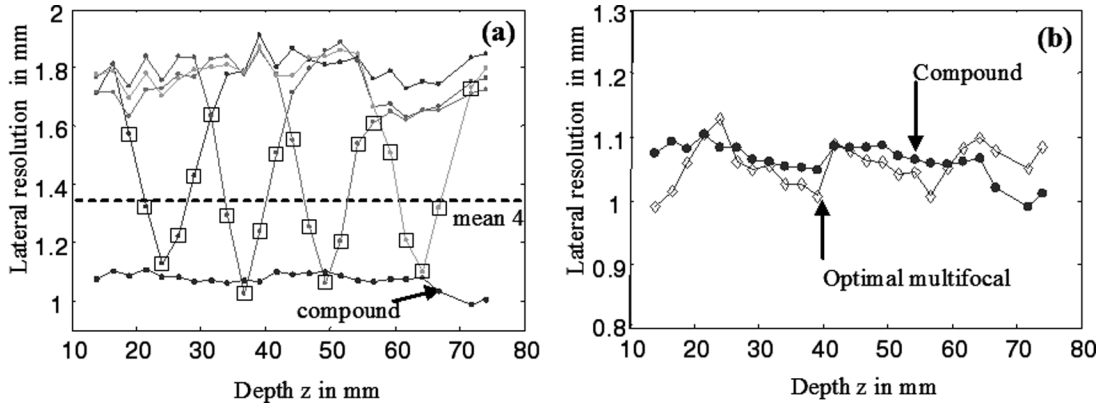
Fig. 6. (a) –10 dB lateral resolution with standard focusing on 4 different depths compared with a compound of 71 plane waves. The squares are the resolution of the multifocus with 4 depths. The line shows the mean value for the multifocal method using the 4 depths. (b) –10 dB lateral resolution with the optimal multifocus method and with the coherent compound approach using 71 plane waves. The lateral resolution is similar in both methods.
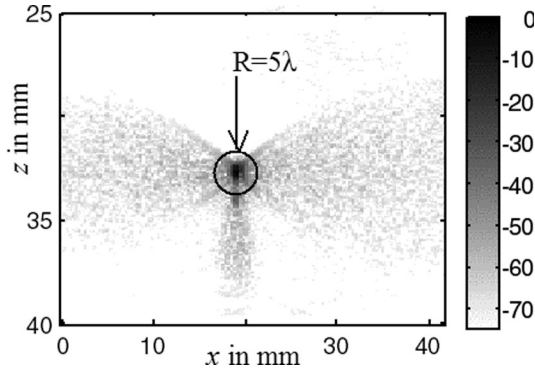

Fig. 7. Example of a PSF function. The color scale in decibels is inversed for the visualization. To measure the contrast, we measured the integral of the energy of the lobes outside a circle of 5λ, and we divided by the total energy of the PSF.

$$s(x, z) = \iint h(x, z, x_1, z_1) o(x_1, z_1) dx_1 dz_1. \qquad (23)$$

The PSF function can be measured experimentally considering that $h(x, z, x_1, z_1)$ is the image of a pointlike object placed in (x_1, z_1). Fig. 7 shows an example of an experimental PSF function; the -10 dB width of the PSF gives directly the lateral resolution.

Fig. 6(a) shows the –10 dB lateral resolution obtained for a standard focusing method with 4 focal distances. The best resolution (~1 mm) is, of course, obtained at each focal depth, but it degrades quite rapidly 1 cm away (~1.8 mm). In the multifocal mode, the image is made by sectors and the resolution is then of the nearest focal depth. The square marks in Fig. 6(a) show the resolution of the 4-focal multifocus image that changes between 1.1 mm in a focal plane to 1.6 mm at equal distance of 2 focal planes. The line at 1.4 mm is the mean resolution of the 4-focal multifocus image.

The coherent compounding method gives a better resolution of 1.1 mm uniformly distributed all over the image. This result is the same as the one obtained using the op-

timal multifocal image. Fig. 6(b) compares the resolution for the coherent compounding method and for the optimal multifocal method. As was predicted, both methods give the same resolution.

B. Contrast in Anechoic Objects

Contrast in anechoic objects describes the ability of the imaging method to detect an anechoic object embedded in a homogeneous scattering medium. Assuming the use of a circular anechoic inclusion R embedded in a homogeneous speckle medium, the contrast can be defined as the difference between the average brightness level in the vicinity of the inclusion and the background level. This contrast difference can be estimated by introducing a point spread function concentric with R and measuring the ratio between the total energy in all the images outside R and the total PSF energy (see Fig. 7).

$$\text{contrast}(x_1, z_1) = 10 \log_{10} \frac{\int\limits_{x,z \notin R} h^2(x_1, z_1, x, z) dx dz}{\int h^2(x_1, z_1, x, z) dx dz}. \qquad (24)$$

The inclusion R is typically chosen as a 5λ diameter circle centered at (x_1, z_1) [28]. Fig. 8(a) shows the contrast level obtained using the standard focal method. At the focal location, the contrast level reaches a minimum value of approximately –32 dB, but it strongly degrades outside the focal zone where it can lose 20 dB. In the multifocal mode, the image is made by sectors and the contrast is then of the nearest focal depth. The square marks in Fig. 8(a) show the contrast of the 4-focal multifocus image; the line at -28 dB is the mean contrast obtained with 4 focal zones. Finally, the compound method gives a uniform contrast of –32 dB versus depth. This optimal contrast level is the same as the one obtained for the optimal multifocus image (again in agreement with the theoretical model); see Fig. 8(b).
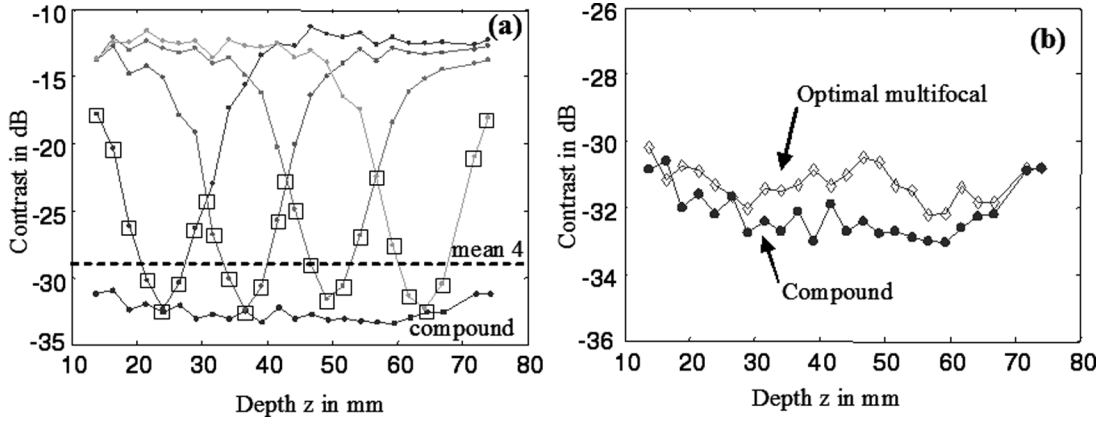
Fig. 8. (a) Contrast with standard focusing at 4 different depths compared with the compound method. The squares are the contrast of the multifocus with the 4 depths. The line shows the mean contrast for a multifocal method using the 4 depths. (b) Contrast of the optimal multifocus method and the coherent compound with 71 plane waves. The contrast is the same for both methods at focal depths.

C. Signal-to-Noise Ratio

Due to ultrasonic attenuation, the amplitude of back-scattered echoes decreases exponentially with depth. Because noise comes mainly from electronics, it can be assumed to be uniform and the signal-to-noise ratio (SNR) decreases exponentially with the imaged depth.

The conventional imaging technique based on line-per-line transmit focusing should maximize the amplitude of echoes reflected by the scatterers located in the focal spot. On the contrary, because the coherent plane-wave imaging method does not rely on transmit focusing, a dramatic attenuation and, consequently, a poor SNR was expected. Fortunately, this expectation proved to be not true. It can even be shown that the coherent compound generates a SNR similar to the one obtained using the optimal multifocus imaging technique.

Assume we try to image a single scatterer at depth z. In this case, a simple analysis of the amplitudes of the incident and backscattered waves enables us to calculate the SNR. The amplitude R of the backscattered signal is proportional to the amplitude $A(z)$ of the pressure that reaches the scatter

$$R = A(z).C, \qquad (25)$$

where C is the proportionality constant.

In the optimal multifocus method, the amplitude at the focal point is given by

$$R_{\text{std}} = p_o g(z_f) e^{-\alpha_{\text{at}} z_f}.C, \qquad (26)$$

where p_o is the pressure amplitude transmitted on the surface of the transducers, $g(z_f)$ is the antenna gain of the array for the chosen focal depth, and α_{at} is the attenuation coefficient.

In the case of a plane wave transmission, there is no antenna gain, and the signal amplitude in the focus is only affected by the attenuation. The backscattered echoes have an amplitude

$$R_{\text{plane}} = p_o e^{-\alpha_{\text{at}} z_f} C. \qquad (27)$$

It is important to note that to generate a plane wave, the array acts as a piston transducer, and it generates a plane wave only in the near field of the array. However, because the Fresnel distance $z_{\text{Fresnel}} = L^2/4\lambda$ is typically 1 m (for a 4 cm aperture array working at 4 MHz), it is clear that the imaging medium is located in the near field of the transmitted field where the signal amplitude for the plane wave is practically constant versus depth and modified only by the attenuation.

The total signal received in the coherent plane compound approach is the addition of the n plane wave signals

$$R_{\text{comp}} = n p_0 e^{-\alpha_{\text{at}} z_f}.C. \qquad (28)$$

The noise is assumed to be mainly due to electronics, and each transmission relies on a statistically independent noise realization. For the multifocus method, a noise η disturbs one single transmit focus realization. For the compound plane wave method, n realizations of this incoherent noise are added, leading to a total noise equal to $\eta\sqrt{n}$. Using (18) to calculate $g(z)$, and (19) to calculate the number of angles n, the rate between the SNR for both methods is then

$$\frac{\text{SNR}_{\text{comp}}}{\text{SNR}_{\text{std}}} = \frac{\sqrt{n}}{g(z_f)} = \sqrt{\frac{L}{2a}}. \qquad (29)$$

Because $2\alpha < L$, this rate is always higher than 1, and the synthetic recombination of the compounded plane waves gives a better SNR than the optimal multifocus image. To confirm this point, the measurement of the SNR is done experimentally using a homogeneous tissue-mimicking phantom. A set of 20 images is acquired in the same conditions. The ultrasonic signal is calculated as the mean of the images and the noise as the standard deviation for
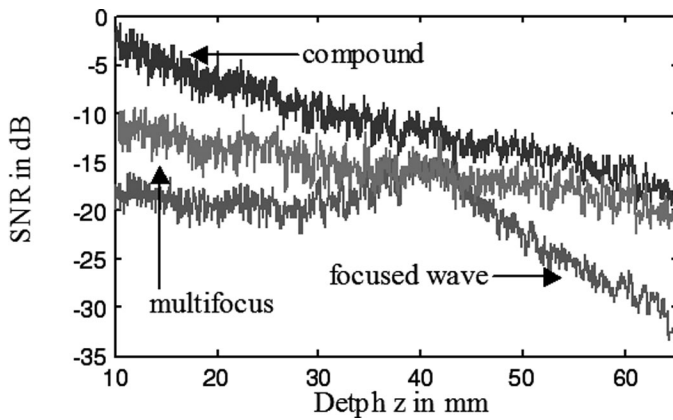
Fig. 9. Measured SNR for the different methods, focused emission at 40 mm depth, the optimal multifocus, and the compound with 71 plane waves. The compound always gives a better SNR.
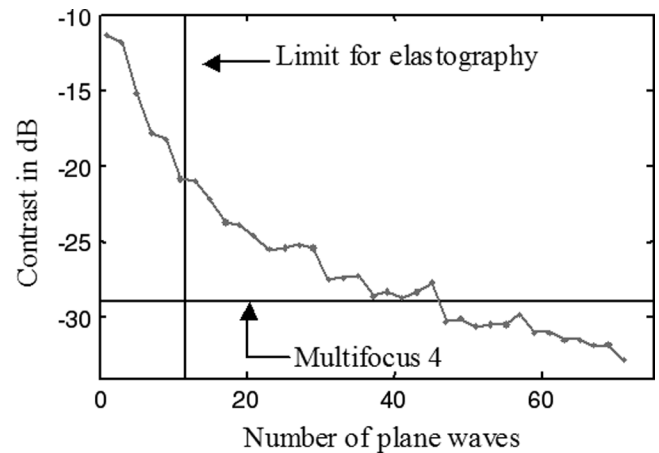

Fig. 10. Contrast in the compound method versus number of plane waves. At 12 angles, we have the limit for the ultrafast echography with a contrast of –22 dB. To obtain the same contrast as in a multifocus method with 4 focal planes, we need 45 angles.

each pixel. Fig. 9 shows the SNR for a compounded image with 71 angles, one focus image, and the optimal multifocus image. The compound method gives always a better SNR than the multifocus image.

This result apparently contradicts the expectation that a focused wave maximizes the signal in the focal point and then increases the SNR. This contradiction is explained by the fact that the focused wave performs one measurement with a good SNR, and the plane-wave compound performs many measurements with poor SNR but the averaged result gives a better SNR than in the focused method.

The combination of low SNR and high frame rate is an interesting property of the coherent compound. It is important to note that it is possible to use coded emissions (chirp codes or Hadamar bases) to reduce the SNR as is done in synthetic aperture methods.

D. Increasing the Frame Rate for Ultrafast Imaging in Transient Elastography

The frame rate is only limited by 2 physical parameters: the speed of sound in tissues that fixes the travel time of the ultrasonic waves in the medium and the ultrasonic attenuation of tissues. The travel time is straightforwardly given by $T_{\text{travel}} = 2\text{Depth}/c$ (as an example, for a scanning depth of 6 cm, it gives a travel time of $T_{\text{travel}} = 80$ μs). Another parameter restricting the frame rate come from the fact that you must wait for a time interval T_{at} after the transmission of the ultrasonic waves before the next emission to ensure the complete attenuation of the backscattered echoes. Assuming an attenuation coefficient α_{at} that is proportional to the frequency, the time T_{at} needed to attenuate the ultrasonic echoes by a 30 dB ratio is $T_{\text{at}} = 30/(\alpha_{\text{at}}cf)$. As an example, with a typical absorption coefficient $\alpha_{\text{at}} = 0.7$ dB/MHz.cm and an imaging frequency $f = 4$ MHz, a time delay $T_{\text{at}} \approx 71$ μs is obtained. It shows that in typical imaging configurations, the travel and attenuation times are quite similar, and a minimal time between 2 insonifications for the previous example is roughly 80 μs. As a direct consequence, the maximal frequency of insonification is limited to $F_{\text{max}} = 12.5$ kHz. Of course, this value must be adjusted for each specific application.

The frame rate for any method that uses n_{ins} insonification to provide one image is $F_{\text{max}}/n_{\text{ins}}$. The plane wave method uses only one insonification, so it provides the fastest imaging modality with a 12.5 kf/s frame rate. The compounded method relies on a lower frame rate because several insonifications are required to provide a single image.

In Fig. 10, we can see the compromise between the number of insonifications in the compound method and the contrast of the image. With 45 angles, we obtain the same contrast as with a 4 plane multifocal method. As we will see later, the maximum frequency of the shear waves used in elastography is 500 Hz [27]; therefore, we need to image the displacement at 1 kHz to take the sampling criteria into account. The limit for elastography is then 12 angles fired at 12 kHz to obtain a final compounded film at 1 kHz with a contrast of 22 dB.

Fig. 11 shows the images for different number of plane waves, we can see an important improvement in the contrast when we increase the number of plane waves.

E. Summary

We demonstrated here that the coherent compounding approach performs as well as the optimal multifocus image but with a significantly higher frame rate. Table I summarizes the principal comparison values for the examples analyzed.

For example, the 4-focal-depth B-mode is comparable to a compound with 45 plane waves, but the latter is 10 times faster. The 12-plane-wave compound has the minimum frame rate for transient elastography, and it is comparable to a standard monofocus image. For a given image quality, the coherent compound method allows a frame rate increase of factor 10 compared with standard scan-
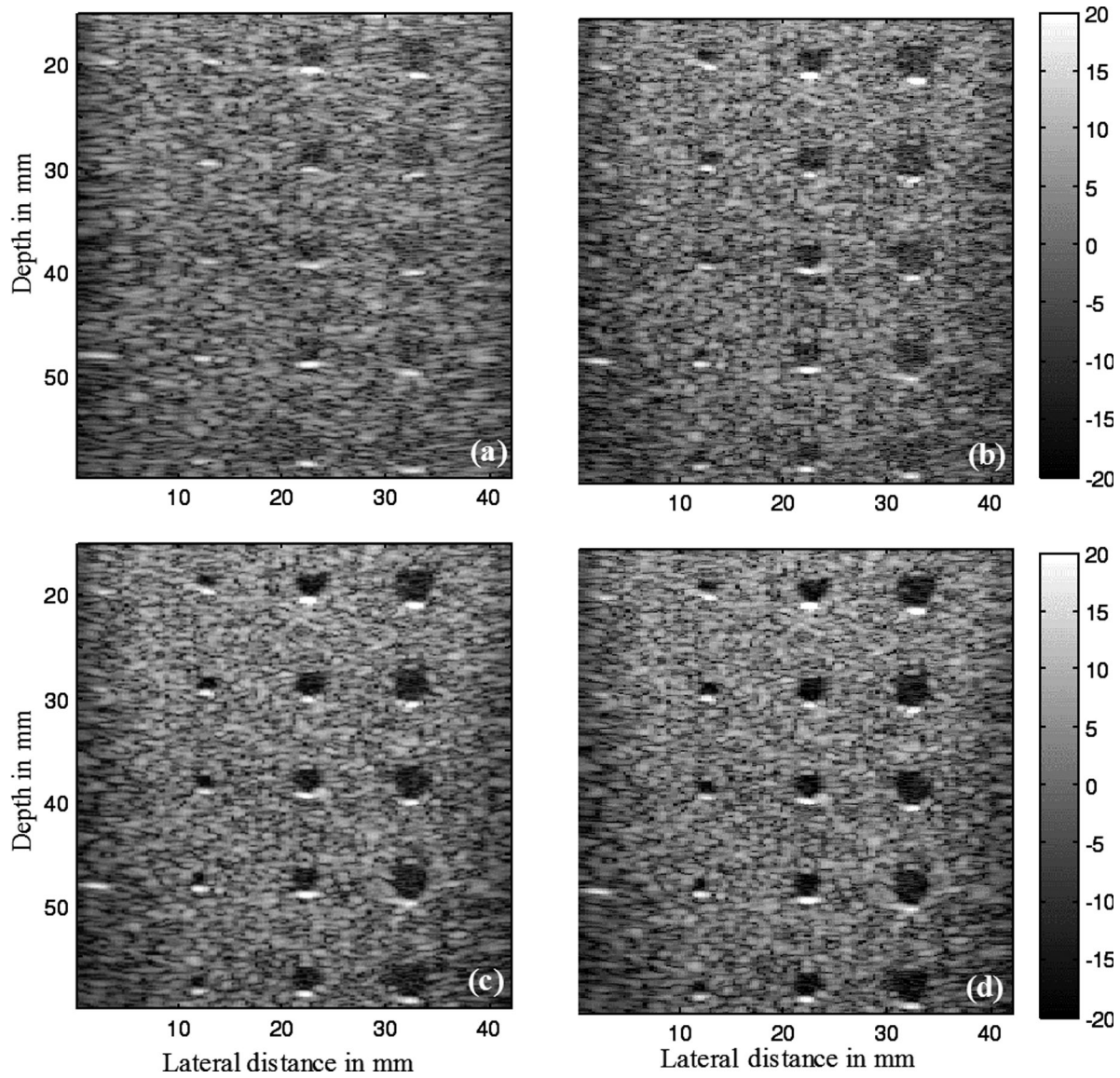
Fig. 11. Images of anechoic objects using different number of plane waves. (a) 1 plane wave, (b) 5 plane waves separated $2°(-4°,-2°,0°,2°,4°)$, (c) 21 plane waves separated 1°, and (d) 45 plane waves separated 0.5°.

TABLE I. QUANTITATIVE COMPARISON FOR THE DIFFERENT METHODS. THE SNR IS RELATIVE TO THE PLANE WAVE.

	Resolution mm	F. rate Hz	Contr. dB	SNR dB	Elastography
Monofocus	1.1 to 1.8	100	12 to 32	18 to 0	No
Multifocus 4	1.35	25	29	18 to 0	No
Multif. Optimal	1.1	8	33	18 to 0	No
Plane wave	1.8	12500	12	0	Yes
Compound 12	1.1	1000	20	11	yes
Compound 45	1.1	270	30	16	no
Compound 71	1.1	176	33	18	no

ning techniques. This value is given for a 128-line image, which corresponds to the typical number of insonified lines on commercial scanners.

The proposed mode is a more efficient way to perform ultrasound imaging than classical line scanning. It can be applied to many imaging modes, such as B-mode, color-flow imaging, or elastography. It requires, however, extremely flexible and powerful system architectures (real-time full parallel processing). Recent progress in CPU capabilities and parallelization makes those architectures achievable. Such a method should provide very promising imaging modes on commercial scanners in the near future. In the next section, we propose investigation of the advantages of implementing the method for transient elastography.

IV. APPLICATION TO TRANSIENT ELASTOGRAPHY

A. The SuperSonic Shear Imaging Modality (SSI)

The basic idea of the transient elastography is that low-frequency (typically 50 to 500 Hz) shear waves propagate in the body at a very low speed (approximately 1 to 10 m/s). Such a low propagation speed enables imaging of tissue displacements induced by the shear wave using compressional ultrasonic waves propagating at 1500 m/s. Nevertheless, to catch this transient propagation of the shear wave, the echographic device must be able to reach very high frame rates (>1000 Hz). The shear waves can be generated either by a mechanical vibrator [7], [8] or by using the radiation force of ultrasonic focused beams. In the approach studied in this section, the generation of a shear wave is achieved by transmitting a focused ultrasonic wave lasting some hundreds of microseconds, the so called "pushing beam." The radiation force of this beam generates a local displacement of tissues in the focal area. This method is used in other elastographic methods like the *acoustic radiation force imaging* [29], [30] or the *vibroacoustography* approach [31]. An important advantage of the pushing beam compared with the mechanical vibrator approach resides in the ability of the operator to shape the vibrating source by simply moving the pushing beam electronically. For example, by increasing the focal depth of the pushing beam at a speed successively faster than the speed of the resulting shear wave, one can generate a "supersonic" source that radiates planar shear waves in a Mach cone (analogous to the sonic boom generated by a supersonic flight). This mode is known as supersonic shear imaging (SSI). The reader interested in this elastography technique can refer to detailed explanations in [10], [11].

Immediately after generating the shear wave, the array switches into an ultrafast imaging mode. The shear wave propagating in the human body has a typical spectrum between 100 to 500 Hz [27]; the echographic frame rate should at least reach 1 kHz to sample correctly the displacements of the tissue. By using speckle correlation between 2 successive echographic images, local tissue displacements can be estimated to obtain a 2-D movie of the transient shear wave propagation. The resolution and quality of the movie is directly linked to the quality of the echographic image. From this movie it is possible to recover the local shear speed at each point of the image by solving the inverse problem of the shear wave propagation [8].

To date, the very high frame rate required to perform the SSI mode was obtained by applying single flat-transmit beams. However, such a single plane-wave transmission results in low-quality images (low SNR, low resolution, and low contrast), penalizing the performances of the tissue displacement estimator. This degradation is particularly important in heterogeneous media with high echogeneicity contrasts due to cluttering, shadowing, or blurring effects. Fig. 12 illustrates these problems. When tissues are moving in a highly echogeneic region, the spatial and temporal
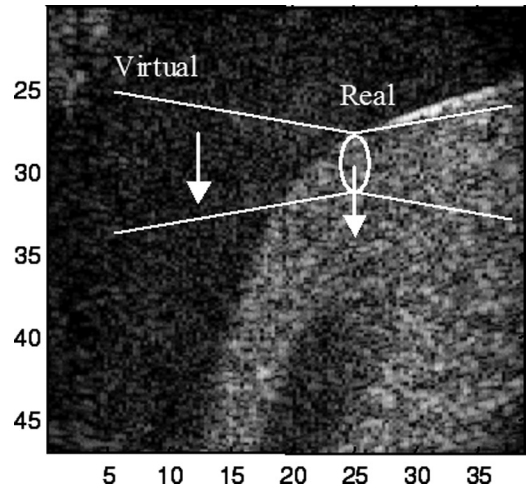

Fig. 12. Single plane wave transmit image of a highly hyper-echogeneic phantom. Due to the side lobes of the point-spread functions in the high-contrast regions that induce artifacts in low-contrast regions, a real displacement in the hyper-echogenic zone generates a virtual displacement in the anechoic zone.

side lobes of the point-spread function induce unwanted motion estimates in neighboring hypoechogeneic and motionless regions. As the image of the anechoic region is dominated or at least distorted by this "diffraction noise" of the point-spread function, its speckle pattern moves even if no physical movement was induced in this area. In human tissues, the acoustic impedance heterogeneities can be very important depending on the organ and can become a major problem for the performances of the displacement estimator. Thus, improving the echographic image quality without sacrificing the very high frame rate could overcome or at least reduce this problem. To evaluate its add-on value, the coherent plane compounding approach described in the previous sections was applied to the SSI mode.

B. Implementation of Coherent Plane-Wave Compounding for Transient Elastography

The time sequence of an experiment combining the remote generation of a pushing line and the ultrafast acquisition of echographic images is summarized in Fig. 13.

During the first 500 μs, the radiation force induced by successive waves focusing at different depths generates the planar shear wave. Then, the echographic device switches into the ultrafast imaging mode. A set of 5 plane waves with different emission angles α_i ($1 \leq i \leq 5$), are fired at a 10 kHz pulse repetition frequency (PRF). By recombining in a coherent way each set of 5 successive plane waves, we produce a compound echographic image every 500 μs (equivalent to a PRF of 2 kHz). Finally, the displacements are measured by 1-D speckle cross-correlation between successive compound images. The shear wave typically needs 50 ms to travel through the entire imaged zone (such as breast or liver). This time is approximately the time needed between 2 images on a conventional ul-
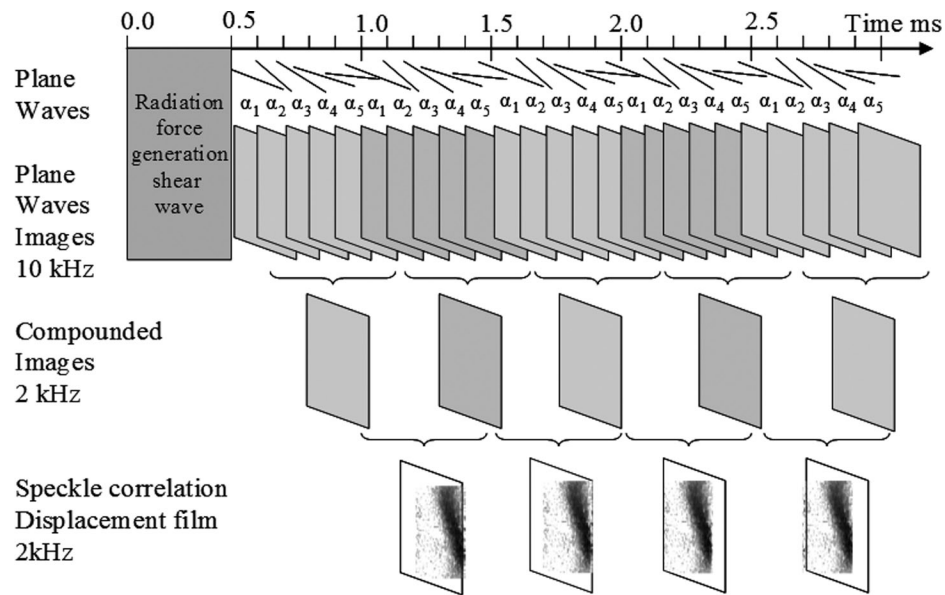
Fig. 13. Chronology of an elastography experiment. In the first 0.5 ms, a monochromatic wave is focused to generate the shear wave by radiation pressure. Five different plane waves are sent at a repetition frequency of 10 kHz. After compounding, we obtained the echographic images at a frequency of 2 kHz. By using speckle correlation, a movie of the shear wave propagation can be computed at a repetition frequency of 2 kHz.
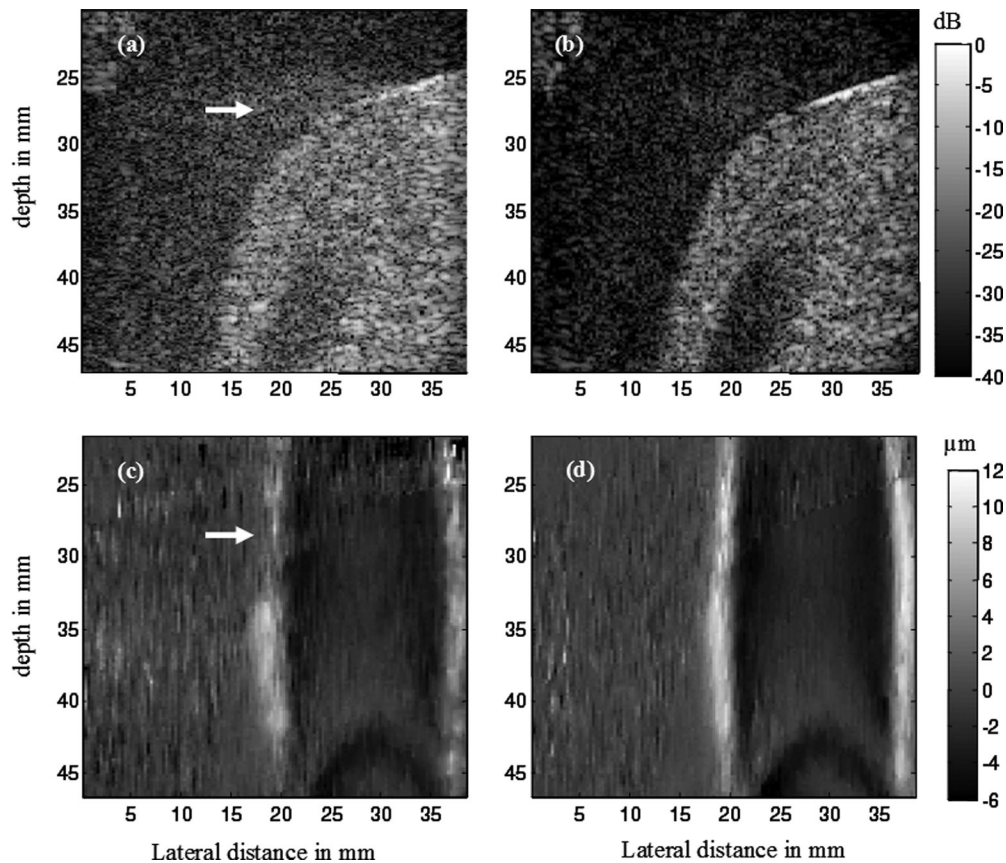

Fig. 14. (a) Plane-wave image of an heterogeneous phantom. (b) Compound image with 14 angles separated 1.5°. The contrast between the object on the right and the background is nearly 20 dB in the compound image. The arrow shows that, in the plane wave image, the side lobes of the echogenic object contaminate the anechoic background. In (c) and (d) is shown displacement of the shear wave at 5 ms with plane waves and compound, respectively. With a single plane wave, the displacement is noisy and underestimated, especially in the zone contaminated by the side lobes of the echogenic object.
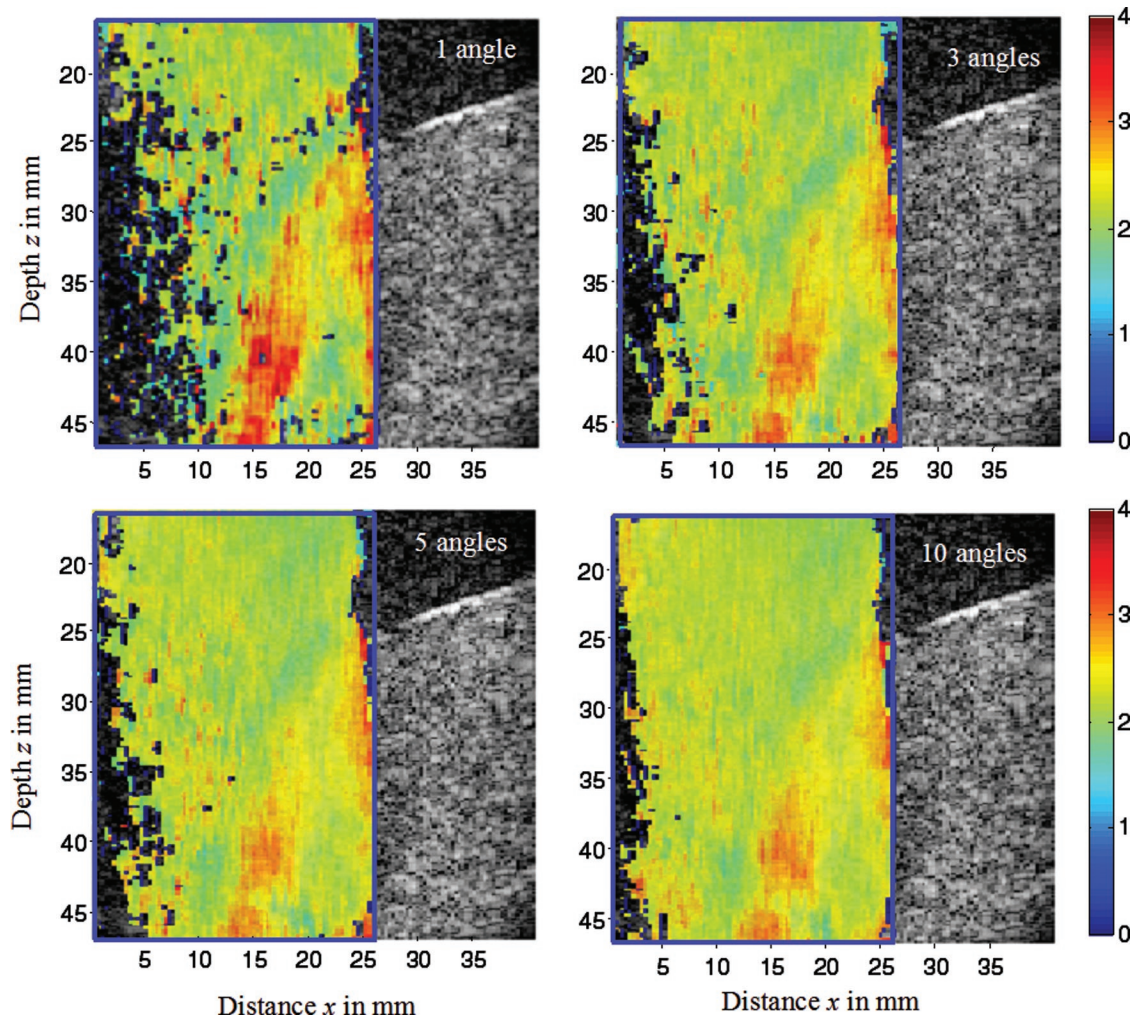
Fig. 15. Elasticity images (expressed in terms of local shear wave speed) calculated in the blue square with 1, 3, 5, and 10 plane waves separated by 1.5°. A color corresponding to the shear speed is superimposed in the points where it is possible to estimate a local speed. We can see an important improvement of the images with the compound.

trasound scanner. It can be noticed that if we want to increase the number of compound angles, it is possible to repeat the experiment and generate an identical shear wave after 50 ms but performing the compound imaging with a set of 5 different angles. The total experiment will then be extended to 100 ms.

B. Efficiency of the Coherent Plane-Wave Compounding for Transient Elastography

Fig. 14(b) shows the compound image obtained with 14 angles in an heterogeneous PVA phantom compared with a single plane-wave transmit approach; see Fig. 14(a). One can notice a hyper-echogeneic area on the right side of the image. The backscattered signals are nearly 20 dB stronger than the ones coming from the left hypoechogeneic zone. Using only one plane-wave transmission, the anechoic zone is contaminated by the side lobes of the point-spread functions from the right side; see the arrow in Fig. 14(a). Contrast and resolution of the single transmit image are quite low. In Fig. 14(c), one can see the tissue displacement induced by the SSI mode obtained using single plane-wave

transmissions. The compound image in Fig. 14(b) relies on a much better contrast and resolution quality. The distortions previously induced in the low-contrast region were cancelled by the coherent compound approach. As an immediate consequence, the displacement estimates using successive compound images are much better, particularly in the transition region between the hyper-echogeneic and the hypo-echogeneic region (marked by the arrow) where the plane wave image was highly perturbed by the side lobes. The variance of tissue displacements estimates is also much better using the coherent compound approach; see Fig 14(d) compared with Fig14(c).

The poor displacement estimation in the plane wave mode is due to the side lobes of the B-mode image. The side lobes are identical for 2 successive images and then they generate a systematic error that biased the displacement estimation even if the correlation coefficient is near 1. At that point, it is not possible to deduce the quality of the estimated displacement from the correlation coefficient.

Finally, the local estimation of the shear-wave speed that permits the building of the Young's modulus map
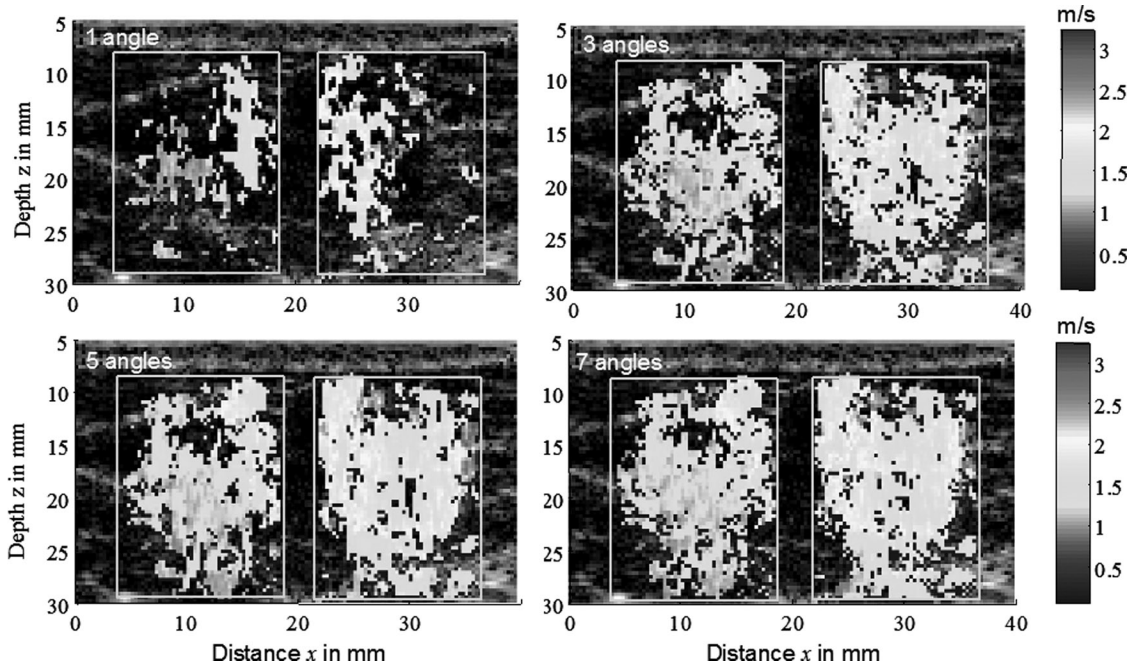
Fig. 16. *In vivo* elastography image of the breast. Using a unique plane wave, the reconstruction is significantly deficient; only 29% of the total image is reconstructed. With 3 angles separated by 1°, (−1°, 0°, 1°) the surface of reconstruction rises to 49%. Using 5 and 7 angles separated by 1°, we obtained a better image that covers 63% and 64% of the total area. The frame rate is 1700 Hz.

can be done using a simple time-of-flight algorithm. It consists in measuring the time Δt needed by the wavefront to travel a small distance Δx (the x-direction is parallel to the front face of the ultrasonic probe). The flight time is estimated by cross-correlating the displacement time profile at location x and at location $x + \Delta x$. The shear-wave speed is directly deduced by calculating $c = \Delta x / \Delta t$. The result obtained using this flight-time algorithm is presented in Fig. 15. A color that corresponds to the local estimates of the shear-wave speed is superimposed on the grayscale B-mode echographic image. Areas without color correspond to regions where the time of flight algorithm failed to recover an estimate because of poor SNR or a poor measurement of the displacement due to the side lobes in the image.

The shear wave is generated along the $x = 30$ mm line. The local speed is calculated in the region of propagation of the shear wave inside the rectangle of Fig. 15.

When increasing the number of compounded plane wave insonifications, the efficiency of the shear-wave speed estimation increases strongly. For the experiment based on single transmit plane waves, more than 18% of the points lead to an inadequate shear wave speed estimation. The number of failing points decreases to 9% with a compounding approach based on 3 plane waves. This number of false points reaches 8.5% with 5 plane waves compounding, and 5.4% for 10 plane waves compounding. The standard deviation of the speed in the homogeneous hypo-echogeneic zone is equal to 0.33 m/s using a single plane wave for transmit, 0.1 m/s using 3 plane waves, 0.08 m/s using 5 plane waves, and finally 0.05 m/s using 10 plane waves. As can be noticed, a reasonable number of 5 plane waves for the coherent compounding approach

leads to a strong improvement of the SSI mode both for the spatial extent of the elasticity image and the accuracy of the local elasticity estimation. This result will be of particular interest in breast-, muscle-, and cardiac-imaging applications where the echographic images suffer strong spatial heterogeneities.

For *in vivo* applications, other problems such as the motion artifacts and minimum frame rate must be analyzed. The *in vivo* applications of the SSI method [9] show that, except for the case of the heart, the motion of the tissue is at very low frequency (lower than 50 Hz). Because the frequency of the shear waves is between 100 to 500 Hz, the low-frequency motion can be easily filtrated. Fig. 16 shows an *in vivo* example of an elastography image of the breast. This study was approved by the French National Committee for the Protection of Patients Participating in Biomedical Research Programs (Authorization No. 2349); the patient provided an informed written consent. The push line was in the middle of the image at $x = 20$ mm; the reconstruction has been performed in the 2 rectangles of the figure. Using a single plane wave, the reconstruction is very deficient; only 29% of the total image is reconstructed. With 3 angles separated 1° (−1°, 0°, 1°) the surface of reconstruction rises to 49%. Using 5 and 7 angles separated by 1°, we obtain a better image that covers 63% and 64% of the total area.

V. CONCLUSION

It is demonstrated in this paper that the coherent summation of flat compounded insonifications is a very promising mode for ultrasound imaging because it provides a

high-end image quality while increasing temporal resolution strongly (around a factor of 10). The classic compromise between temporal resolution and image quality is broken, and new perspectives can be envisioned: Fast B and color modes could be of significant interest for cardiac and 3-D applications. In transient elastography, the coherent plane-wave compound approach allows a gain of approximately 10 dB in contrast and a spatial resolution that is two times better than single flat insonifications.

APPENDIX A

In the coherent compound, we use n_k plane waves of inclination $\alpha_i, i = 1.. \ n_k$, we superimpose the images after the beamforming, and then the emission and reception stages are mixed. In this appendix, we separate the 2 stages formally to compare the compound and the multifocus method.

Let $p(x,z,t)$ be the pressure wave sent by the ultrasonic array. This wave is backscattered by the medium and registered by the transducers. Because all these filters are linear and time invariant, the *RF* signals backscattered to the array can be expressed as

$$
\begin{aligned}
RF(x_2, t) &= \int p(x_1, t) \otimes h(x_1, x_2, t) dx_1 \\
&= \iint p(x_1, t') h(x_1, x_2, t - t') dt' dx_1,
\end{aligned} \tag{A1}
$$

where h is a linear filter that takes into account the transducer response, the diffraction, and the backscattering of the medium.

To make a point (x,z) of the image, we perform the beamforming in reception as it was explained in (2)

$$
s(x,z) = \int RF(x_2, \tau(x, z, x_2)) dx_2, \tag{A2}
$$

where the delays τ are different for plane and focused wave. We do not write the integral limits to simplify the notation.

By replacing (A1) in (A2), we obtain

$$
s(x,z) = \iiint p(x_1, t') h(x_1, x_2, \tau(x, z, x_2) - t') dt' dx_1 dx_2. \tag{A3}
$$

The delays τ can be divided in 2 components,

$$
\tau(x, z, x_2) = \tau_e(x, z) + \tau_r(x, z, x_2), \tag{A4}
$$

where τ_e corresponds to the travel from the transducers to the point (x,z) that is

$$
\begin{cases}
\tau_{ec}^{\ i} = (z \cos \alpha_i + x \sin \alpha_i)/c & \text{plane wave} \\
\tau_{ef} = z/c & \text{focused wave}
\end{cases}, \tag{A5}
$$

and τ_r is the return travel time from the point (x,z) to the point x_2 in the array, this delay is the same for both methods

$$
\tau_r = \frac{1}{c}\sqrt{z^2 + (x - x_2)^2}. \tag{A6}
$$

Replacing (A4) in (A3) and integrating with a new variable $t'' = t' - \tau_e$, we can rearrange the terms of the emission and reception as

$$
\begin{aligned}
s(x,z) = \iiint & p(x_1, t'' + \tau_e(x, z)) \\
& \times h(x_1, x_2, \tau_r(x, z, x_2) - t'') dx_1 dx_2 d''.
\end{aligned} \tag{A7}
$$

The first term is a delayed emission wave; the second term is only linked to the reception because it has the backscattering and the reception delays. With this separation between emission and reception, it is possible to compare the compound and focused methods.

In the compound method, we have $p_c^{\ i}$ plane wave emissions. For each plane wave, we build a partial image $s_c^{\ i}$, and the compounded image is the addition of these partial images. Using (A7), we determine that the compounded image is

$$
\begin{aligned}
s_c(x,z) = \iiint & \left[\sum_i p_c^{\ i}(x_1, t'' + \tau_{ec}^{\ i}(x, z)) \right] \\
& \times h(x_1, x_2, \tau_r(x, z, x_2) - t'') dx_1 dx_2 dt''.
\end{aligned} \tag{A8}
$$

The focal method gives an image given directly by (A7) with the delays τ_{ef}

$$
\begin{aligned}
s(x,z) = \iiint & p(x_1, t'' + \tau_{ef}(x, z)) \\
& \times h(x_1, x_2, \tau_r(x, z, x_2) - t'') dx_1 dx_2 dt''.
\end{aligned} \tag{A9}
$$

Comparing (A8) with (A9), we observe that the term $h(x_1, x_2, \tau_r - t'')$ is the same for both methods because the reception delays are the same. If we demonstrate that the delayed emissions are the same,

$$
\sum_i p_c^{\ i}(x_1, t + \tau_{ec}^{\ i}(x, z)) \underset{?}{=} p_f(x_1, t + \tau_{ef}(x, z)). \tag{A10}
$$

We can conclude that both methods produce the same image. This calculation is done in Section II-D. Another interpretation of (A8) is that the image in a point (x,z) with the compound method can be produced with a unique emission wave $\sum_i p_c^{\ i}(x_1, t + \tau_{ec}^{\ i}(x, z))$, that is the synthetic wave of the compound method.

APPENDIX B

If we send a cylindrical wave that focuses on the point $(0, z_f)$, for a monochromatic wave the focal spot is a func-

tion $\mathrm{sinc}(xak_0/z_f)$, as in (14) that we can write in function of the temporal frequency $\omega = ck_0$:

$$p(x) = B\mathrm{sinc}\left(x\,\frac{\omega a}{cz_f} \right). \tag{B1}$$

If the focused wave is a wideband pulse with a temporal spectrum $B(\omega)$, the focal spot is the integration of (B1) in the temporal frequencies

$$p(x) = \int_{-\infty}^{+\infty} B(\omega)\mathrm{sinc}\left(x\,\frac{\omega a}{cz_f} \right)d\omega. \tag{B2}$$

The spatial Fourier transform of (B2) is

$$P(k_x) = \int_{-\infty}^{+\infty} B(\omega)\mathrm{rec}\left(k_x\,\frac{cz_f}{\omega a} \right)d\omega, \tag{B3}$$

where $\mathrm{rec}(y)$ is the rectangle function (one if $|y| < 1$ and zero elsewhere).

For a positive k_x we can calculate this integral as

$$P(k_x) = \int_{k_x cz_f/a}^{+\infty} B(\omega)d\omega. \tag{B4}$$

We can illustrate this last equation calculating the integral for different cases. For a monochromatic wave, the spectrum is a Dirac's delta $B(\omega) = \delta(\omega - \omega_0)$, and the integral (B4) recreates the rectangle function

$$P_{\mathrm{monoc}}(k_x) = \mathrm{rec}\left(\frac{k_x z_f}{k_0 a} \right). \tag{B5}$$

If $B(\omega)$ is a Gaussian impulsion of bandwidth $\Delta\omega$ centered in ω_0

$$B(\omega) = \frac{1}{\Delta\omega\sqrt{2\pi}}\exp\left(\frac{-(\omega - \omega_0)^2}{2\Delta\omega^2} \right). \tag{B6}$$

The integration (B3) gives the error function

$$P_{\mathrm{Gauss}}(k_x) = \Phi\left(\frac{|k_x|\frac{z_f}{a} - k_0}{\Delta k} \right), \tag{B7}$$

with $\Delta k = \Delta\omega/c$, in this case the edges of the rectangle are smoothened in a section Δk as we can see in Fig. 5.

References

[1] B. Delannoy, R. Torgue, C. Bruneel, and E. Bridou, "Ultrafast electronical image reconstruction device" in *Echocardiology*, vol. 1, C. T. Lancee, Ed. (The Hague: Nijhoff, 1979), ch. 3, pp. 447–450.

[2] B. Delannoy, R. Torgue, C. Bruneel, E. Bridoux, J. M. Rouvaen, and H. LaSota, "Acoustical image reconstruction in parallel-processing analog electronic systems," *J. Appl. Phys.*, vol. 50, pp. 3153–3159, May 1979.

[3] D. Shattuck, M. Weinshenker, S. Smith, and O. Von Ramm, "Explososcan: A parallel processing technique for high speed ultrasound imaging with linear phased arrays," *J. Acoust. Soc. Am.*, vol. 75, no. 4, p 1273–1282, Apr. 1984.

[4] S. W. Smith, H. G. Pavy, and O. T. von Ramm, "High-speed ultrasound volumetric imaging system. I. Transducer design and beam steering," *IEEE Trans. Ultrason. Ferroelectr. Freq. Control*, vol. 38, no. 2, pp. 100–108, Mar. 1991.

[5] O. T. von Ramm, S. W. Smith, and H. G. Pavy, "High-speed ultrasound volumetric imaging system. II. Parallel processing and image display," *IEEE Trans. Ultrason. Ferroelectr. Freq. Control*, vol. 38, no. 2, pp. 109–115, Mar. 1991.

[6] L. Sandrin, S. Catheline, M. Tanter, X. Hennequin, and M. Fink, "Time resolved pulsed elastography with ultrafast ultrasonic imaging," *Ultrason. Imaging*, vol. 21, pp. 259–272, Oct. 1999.

[7] L. Sandrin, S. Catheline, M. Tanter, C. Vinçonneau, and M. Fink, "2D transient elastography," *Acoust. Imaging*, vol. 25, pp. 485–492, Jan. 2000.

[8] L. Sandrin, M. Tanter, S. Catheline, and M. Fink, "Shear modulus imaging using 2D transient elastography," *IEEE Trans. Ultrason. Ferroelectr. Freq. Control*, vol. 49, no. 4, pp. 426–435, Apr. 2002.

[9] J. Bercoff, S. Chaffai, M. Tanter, L. Sandrin, S. Catheline, M. Fink, J.-L. Gennisson, and M. Meunier, "In vivo breast tumors detection using transient elastography," *Ultrasound Med. Biol.*, vol. 29, no. 10, pp. 1387–1396, 2003.

[10] J. Bercoff, M. Tanter, and M. Fink, "Sonic boom in soft materials: The elastic Cerenkov effect," *Appl. Phys. Lett.*, vol. 84, no. 12, pp. 2202–2204, Mar. 2004.

[11] J. Bercoff, M. Tanter, and M. Fink, "Supersonic shear imaging: A new technique for soft tissues elasticity mapping," *IEEE Trans. Ultrason. Ferroelectr. Freq. Control*, vol. 51, no. 4, pp. 396–409, Apr. 2004.

[12] J.-Y. Lu and J. F. Greenleaf, "Pulse-echo imaging using a nondiffracting beam transducer," *Ultrasound Med. Biol.*, vol. 17, no. 3, pp. 265–281, 1991.

[13] J.-Y. Lu and J. F. Greenleaf, "Ultrasonic nondiffracting transducer for medical imaging," *IEEE Trans. Ultrason. Ferroelectr. Freq. Control*, vol. 37, pp. 438–447, Sep. 1990.

[14] J.-Y. Lu and J. F. Greenleaf, "Experimental verification of nondiffracting X waves," *IEEE Trans. Ultrason. Ferroelectr. Freq. Control*, vol. 39, pp. 441–446, May 1992.

[15] J.-Y. Lu, "2-D and 3-D high frame rate imaging with limited diffraction beams," *IEEE Trans. Ultrason. Ferroelectr. Freq. Control*, vol. 44, pp. 839–856, Jul. 1997.

[16] J.-Y. Lu, "Experimental study of high frame rate imaging with limited diffraction beams," *IEEE Trans. Ultrason. Ferroelectr. Freq. Control*, vol. 45, pp. 84–97, Jan. 1998.

[17] J. Cheng and J. Y. Lu, "Extended high frame rate imaging method with limited diffraction beams," *IEEE Trans. Ultrason. Ferroelectr. Freq. Control*, vol. 53, pp. 880–899, May 2006.

[18] M. Berson, A. Roncin, and L. Pourcelot, "Compound scanning with an electrically steered beam," *Ultrason. Imaging*, vol. 3, no. 3, pp. 303–308, 1981.

[19] S. K. Jespersen, J. E. Wilhjelm, and H. Sillesen, "Multi-angle compound imaging," *Ultrason. Imaging*, vol. 20, pp. 81–102, Apr. 1998.

[20] R. R. Entrekin, B. A. Porter, H. H. Sillesen, A. D. Wong, P. L. Cooperberg, and C. H. Fix, "Real-time spatial compound imaging: Application to breast, vascular, and musculoskeletal ultrasound," *Semin. Ultrasound CT MR*, vol. 22, pp. 50–64, Feb. 2001.

[21] F. Forsberg, "Ultrasonic biomedical technology; marketing versus clinical reality," *Ultrasonics*, vol. 42, pp. 17–27, Apr. 2004.

[22] T. K. Song and J. H. Chang, "Synthetic aperture focusing method for ultrasound imaging based on planar waves," U.S. Patent 0125628, Jul 3, 2003.

[23] J. Jensen, O. Holm, L. J. Jerisen, H. Bendsen, S. I. Nikolov, B. G. Tomov, P. Munk, M. Hansen, K. Salomonsen, J. Hansen, K. Gormsen, H. M. Pedersen, and K. L. Gammelmark, "Ultrasound research scanner for real-time synthetic aperture data acquisition," *IEEE Trans. Ultrason. Ferroelectr. Freq. Control*, vol. 52, no. 5, pp. 881–891, May 2005.

[24] T. Misaridis and J. A. Jensen, "Use of modulated excitation signals in medical ultrasound. Part III: High frame rate imaging," *IEEE Trans. Ultrason. Ferroelectr. Freq. Control*, vol. 52, no. 2, pp. 208–219, Feb. 2005.

[25] M. Tanter, J. Bercoff, L. Sandrin, and M. Fink, "Ultrafast compound imaging for 2D motion vector estimation: Application to transient elastography," *IEEE Trans. Ultrason. Ferroelectr. Freq. Control*, vol. 49, no. 10, pp. 1363–1374, Oct. 2002

[26] G. S. Kino, *Acoustic Waves, Devices Imaging and Analog Signal Processing.* Upper Saddle River, NJ: Prentice Hall, 1987, p. 191.

[27] T. Deffieux, G. Montaldo, M. Tanter, and M. Fink, "Shear wave spectroscopy of human soft tissues for in vivo quantification of the viscoelasticity," *IEEE Trans. Med. Imaging,* to be published.

[28] K. F. Üstüner and G. L. Holley, "Ultrasound imaging system performance assessment," AAPM 45th Annu. Meeting, 2003. [Online] Available: http://www.aapm.org/meetings/03AM/pdf/9905-9858. pdf.

[29] K. R. Nightingale, M. L. Palmeri, R. W. Nightingale, and G. E. Trahey, "On the feasibility of remote palpation using acoustic radiation force," *J. Acoust. Soc. Am.*, vol. 110, no. 1, pp. 625–634, Jul. 2001.

[30] K. Nightingale, M. Soo, R. Nightingale, and G. Trahey, "Acoustic radiation force impulse imaging: *In vivo* demonstration of clinical feasibility," *Ultrasound Med. Biol.*, vol. 28, no. 2, pp. 227–235, Feb. 2002.

[31] M. Fatemi and J. F. Greenleaf, "Ultrasound-stimulated vibroacoustic spectrography," *Science*, vol. 280, pp. 82–85, Apr. 1998.

Gabriel Montaldo was born in 1972 in Montevideo, Uruguay. He received the Ph.D. degree in physics from the Universidad de la Republica, Uruguay, in 2001. Since 2002 he has worked in the Laboratory Ondes et Acoustique at the Ecole Supérieure de Physique et de Chimie Industrielles de la Ville de Paris (ESPCI).

His principal research includes applications of the time-reversal process to adaptive focusing in heterogeneous media and biomedical applications of ultrasound and elastography. He holds 5 patents in the ultrasound domain and has published more than 20 reviewed articles.

Mickaël Tanter received the Diplôme d'Ingénieur (High Engineering Degree) in electronics from Ecole Supérieur d'Electricité in 1994 and the Diplôme d'Etudes Approfondies (M.Sc. degree) from Paris VII University in physics and acoustics. In 1999, he received the Ph.D. degree in applied physics from the University of Paris VII. From 2000 to 2005, he was a research associate professor of CNRS at the Laboratory Ondes et Acoustique at ESPCI in Paris and joined the French Institute for Medical Research (INSERM) as a Research Professor in 2006, and currently holds that position. He is also heading the team "Wave Physics for Medicine" at the Laboratoire Ondes et Acoustique, ESPCI, Paris, France.

His main activities are centered around the development of new medical imaging and therapy techniques. His current research interests cover a wide range of topics including ultrasonic therapy and echographic imaging of the brain, elasticity imaging of organs using ultrafast scanners, and compact lithotripers. He is the recipient of 15 patents in the field of ultrasound imaging. He is the author of more than 70 technical peer-reviewed papers. He is a co-founder and shareholder of the SuperSonic Imagine company in the field of ultrasonic medical imaging and therapy.

Jérémy Bercoff was born in August 1977 in Paris, France. He received, in 2001, the engineer degree from the Ecole Supérieure de Physique et de Chimie de Paris (ESPCI) with a specialization in physics. In 1999, he worked at ATL Ultrasound, a Philips Medical System company based on Seattle, WA, on the development of echographic systems. In 2004, he received the Ph.D. degree in physics (acoustics) from the University of Paris VII for his work on ultrafast imaging and shear wave propagation in soft tissues for cancer detection. After a post-doctoral position at the Laboratoire Ondes et Acoustique in 2005, he joined SuperSonic Imagine as a key ultrasound engineer for the development and implementation of the elastography imaging mode.

Nicolas Benech was born in Montevideo, Uruguay in February 1976. He received a physics degree in 2000 from the Science Faculty, Universidad de la República, Uruguay. He received the M.S. and Ph.D. degrees in acoustics in 2004 and 2008, respectively, from the same university.

Now he is an assistant professor at the Science Faculty, Universidad de la República. His current research interests are in the areas of elastography, ultrasonic medical imaging, signal processing, tissue biomechanics, and physical acoustics.
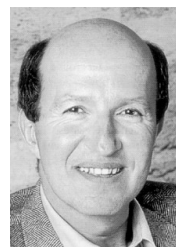
Mathias Fink received the M.S. degree in mathematics from Paris University, France in 1967 and the Ph.D. degree in solid state physics in 1970. Then he moved into medical imaging and received the Doctorat es-Sciences degree in 1978 from Paris University in the area of ultrasonic focusing with transducer arrays for real-time medical imaging.

Dr. Fink is a professor of physics at the Ecole Supérieure de Physique et de Chimie Industrielles de la Ville de Paris (ESPCI), Paris, France, and at Paris VII University (Denis Diderot), France. In 1990 he founded the Laboratoire Ondes et Acoustique at ESPCI. In 2002, he was elected to the French Academy of Engineering and in 2003 to the French Academy of Science.

His current research interests include medical ultrasonic imaging; ultrasonic therapy; nondestructive testing; underwater acoustics; telecommunications; seismology; active control of sound and vibration; analogies between optics, quantum mechanics, and acoustics; wave coherence in multiply scattering media; and time reversal in physics. He has developed different techniques in acoustic imaging (transient elastography), wave focusing in inhomogeneous media (time-reversal mirrors), speckle reduction, and in ultrasonic laser generation. He holds 40 patents, and he has published more than 300 articles.